## The second European Conference on the Structural Integrity of Additively Manufactured Materials

# Effects of hybrid post-treatments on fatigue behaviour of notched LPBF AlSi10Mg: experimental and deep learning approaches

E. Maleki [1*], S. Bagherifard [1], F. Sabouri [1], M. Guagliano [1]

[1] Department of Mechanical Engineering, Politecnico di Milano, Milano, Italy

## Abstract

Laser powder bed fusion (LPBF) as one of the widely used technologies of additive manufacturing (AM), has a high capability to produce complex geometries such as notched parts in a layer-by-layer manner. LPBF parts in their as built state have inhomogeneous and anisotropic microstructure and poor surface quality. Post-treatments can play a key role in modulating these imperfections. In this study, the effects of four different post-treatments including heat treatment, shot peening and electro-chemical polishing as well as their combination as hybrid treatment were investigated on microstructure, surface and mechanical properties and finally fatigue behaviour of the LPBF V-notched AlSi10Mg samples. Afterward, a deep learning based approach was employed for modelling the fatigue behaviour via artificial neural network. Surface roughness, surface modification factor, hardness, residual stress and porosities were considered as inputs and fatigue life was considered as the output. Model function of the network was generated and the relevant parametric and sensitivity analyses were performed. The results indicated the importance of surface related properties and the notable effect of the surface post-treatments in enhancing the fatigue performance of the LPBF material.

* Corresponding author. Tel.: +393479991540
*E-mail address:* erfan.maleki@polimi.it

## 1. Introduction

Laser powder bed fusion (LPBF) as one the widely use additive manufacturing (AM) technologies has gained considerable attention to fabricate verities of components with complex geometries in different industries such as aviation, automotive, medical, etc. in an economical fashion compared to conventional subtractive manufacturing methods as reported by (DebRoy et al., 2018; Gardan, 2016). Due to the layer-by-layer nature of LPBF and the relevant complex physical phenomena occurring during the deposition of the feed-stock materials, these parts inherently have a wide range of internal and surface defects as described by (Erfan Maleki et al., 2021; Yadroitsev and Smurov, 2011). Generally, metallic LPBF materials have anisotropic microstructure (Herzog et al., 2016) and they are specified with different internal defects such as trapped voids, and lack of fusion (Ferro et al., 2020), residual stresses (Mfusi et al., 2019; Mukherjee et al., 2017), and very poor surface qualities (Hamidi Nasab et al., 2018). These defects have detrimental effects on the mechanical and fatigue behavior of these materials as mentioned by (Balachandramurthi et al., 2018; Lewandowski and Seifi, 2016; E. Maleki et al., 2021b). Dealing with poor surface quality of AM materials, very rough surfaces with extremely irregular morphologies caused by partially melted feed-stock, spatters and balling effects can be characterized on the as-built state of the fabricated AM parts especially in the ones built by LPBF (Hamidi Nasab et al., 2018; Li et al., 2012; Sames et al., 2016; Zhang et al., 2018). These surface defects are affected by different factors of feed-stock (powder) material specifications, design and geometry of part and also the considered process parameters of the LPBF (E. Maleki et al., 2021a). Considering these surface imperfections and their detrimental effects, applying surface post-treatments such as chemical and mechanical surface treatments and can play a key role in modulating this issue (AlMangour and Yang, 2016; E. Maleki et al., 2021c). On the other hand, alternative approaches based on artificial intelligence (AI) such as neural networks (NN) has revealed considerable capabilities in prediction, optimization and analyzing of different complex phenomena in various fields of science and engineering (Maleki and Farrahi, 2018; Maleki and Unal, 2019; Maleki et al., 2017). NNs have been also used in the field of AM, in particular for fatigue behavior prediction and analyses (Chen and Liu, 2021; Qi et al., 2019; Zhan and Li, 2021). Generally, a NN has three main layers of input, hidden and output (Maleki and Unal, 2020a). Shallow neural network (SNN), as the primary generation of artificial neural networks have 1 or 2 hidden layers, which are mostly trained by back-propagation (BP) algorithm (Maleki et al., 2018; Maleki and Maleki, 2015). In order to develop SNN, large number of data set is required which can be quite limiting in lots of costly phenomena (Livingstone et al., 1997). By using deep learning methods including restricted Boltzmann machine (RBM) and deep belief network (DBN) presented by Hinton et al. (Hinton et al., 2006; Hinton and Salakhutdinov, 2006) as remarkable improvements obtained in the field of NNs, it is feasible to develop deep neural network (DNN) using greedy layer-wised with pre-training via a small data set. Other approaches for pre-training of DNN such as stacked auto-encoder (SAE) were later presented, to make the development of DNN possible with smaller data set with very high efficiency in accuracy of predicted results as reported by (Bengio et al., 2007; Feng et al., 2019; Liu et al., 2018; Wang et al., 2017).

Herein, we studied the effects of four different post-treatments including heat treatment (HT), shot peening (SP) and electro-chemical polishing (ECP) treatments as well as their combination as hybrid treatments, on microstructure, mechanical properties and fatigue behavior of LPBF V-notched AlSi10Mg samples. Comprehensive experimental tests including microstructural characterization, porosity and surface morphology analyses as well as mechanical characterization including hardness and residual stresses measurement and rotating bending fatigue tests were performed on the as-built and heat treated samples before and after applying SP and ECP treatments. Afterward, a deep learning based approach was used for modelling the fatigue behaviour via artificial neural network. Surface roughness, surface modification factor, surface hardness, surface residual stresses, relative density, yield strength and elongation were considered as inputs and fatigue life was regarded as the output of the developed

network. NN modelling was performed by developing different SNN, DNN and stacked auto-encoder assigned deep (SADNN) neural networks for analyzing and optimization of the fatigue behavior of the treated samples.

## 2. Experimental procedure

Following the authors' previous work (Maleki et al., 2022), which studied the effects of different post-processing methods of HT, SP and their combination as a hybrid treatment on fatigue strength of V-notched LPBF AlSi10Mg samples, same material and samples were used in this study. Gas atomized spherical powder of AlSi10Mg with mean diameter of 46.65 μm was used for LPBF samples manufacturing. The samples were built via SLM 500 HL systems with Yttrium fiber lasers and process parameters of spot diameter of 78 μm, laser power of 350 W, and scan speed of 1150 mm /s, layer thickness of 50 μm and hatch distance of 170 μm were employed. The samples were built vertically with scanning strategy of 67° rotation between the layers and also contour remelting was considered. Cylindrical samples with V-shaped notches were fabricated. Fig. 1 reveals the shape and size of the notched fatigue samples and the fabricated sample in its as-built state.
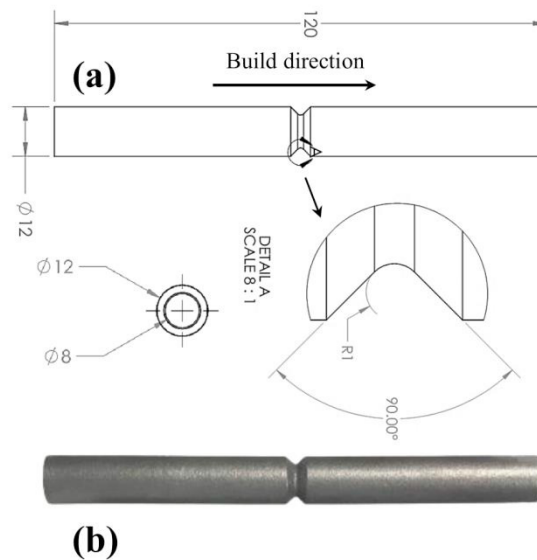


Fig.1. (a) Shape and size of the cylindrical V-notched fatigue sample with R1 notch root radius. (b) As-built state of the fabricated sample; adopted from (Maleki et al., 2022).

Different post-treatments were performed on the samples. Firstly, HT was applied aimed at modifying the microstructural and residual stresses. However, the other two including SP and ECP were applied to modify the surface imperfections. T6 thermal treatment was carried out to half of the produced samples according to the time and temperature intervals reported by (Bagherifard et al., 2018). SP treatment was applied using air blast shot peening equipment with steel impacting media. Table 1 represents the details of considered SP process which applied on both as-built and heat treated samples. Almen intensity was obtained based on the SAE J443 standard (SAE International, 2010).

Table 1. Details of the applied SP treatment on LPBF AlSi10Mg samples

| SP treatment | Shot material | Shot hardness (HRC) | Shot standard category | Shot diameter (mm) | Almen intensity (A 0.001 inch) | Surface coverage (%) |
|---|---|---|---|---|---|---|
| SP1 | Steel | 50 | S 170 | 0.43 | 10 | 100 |

In addition, ECP was carried out using bath of 400 mL solution with 94% Acetic acid ($CH_3COOH$)+6% Perchloric ($HClO_4$) acid at voltage of 15 V and duration time of 240 s, on as-built, heat treated and shot peened series.

Considering the as-built (AB) sample and applied treatments, eight sets of samples including AB, AB+HT, AB+SP, AB+ECP, AB+HT+SP, AB+HT+ECP, AB+SP+ECP and AB+HT+SP+ECP were considered to investigate the sole influence of each post-treatment as well as their hybrid conditions.

In order to perform microstructural characterization, firstly, samples were cut in longitudinal and transversal sections with respect to the build direction. Final step of polishing carried out with silica suspensions. The polished cross-sections were chemically etched for 20 s in Keller's reagent. The microstructural characterization was carried out using two methods of optical microscopy (OM) via a Nikon Eclipse LV150NL optical microscope and a high resolution field-emission scanning electron microscopy (FESEM) using Zeiss Sigma 500 VP equipped with electron backscattered diffraction (EBSD) and the AZtecHKL software was used to process the EBSD data.

SEM based analyses were employed for porosity measurements on the notch area of the samples considering *yz*-plane. Three back scattered electron SEM (BSE-SEM) images were taken from random areas and ImageJ software (Schneider et al., 2012) was employed for analyzing the BSE-SEM micrographs by binerzing the images to black and white.

Surface roughness measurements were carried out via Mahr Perthometer (PCMESS 7024357) equipped with MFW 250 probe with a tip diameter of 5 μm. EN ISO 4287 standard (EN ISO 4287, 1997) was followed for sampling and cut-off wavelengths and the filtering parameters. Three samples were considered for each series and three measurements were applied on random surface areas of each and roughness parameter of arithmetic mean ($R_a$) was obtained for each set. Surface morphologies of the as-built and treated samples were investigated via a Zeiss EVO50 SEM on the notch area.

Microhardness tests were performed on surface of the samples using a Leica WMHT30A micro Vickers hardness tester using load of 25 gf and dwell time of 15 s for each 5 applied indentations.

X-ray diffraction (XRD) was used to obtain the residual stresses on the top surface of the samples in each set. AST X-Stress 3000 portable X-ray diffractometer with CrKα radiation, λK alpha 1 = 2.2898 Å, irradiated area of 4 mm diameter, and $\sin^2(\psi)$ method, was used. Diffraction angle (2θ) of 139° corresponding to {311}-reflex was scanned with a total of 7 Chi tilts between 45° and −45° along three rotations of 0°, 45°and 90°. Fatigue behavior of LPBF V-notched AlSi10Mg were analyzed via rotating bending fatigue tests at a stress ratio of R=−1 at room temperature via a Italsigma equipment with rotational speed around 2500 rpm and fixed amplitude stress of 110 MPa with a run-out limit set to $6 \times 10^6$ cycles for all sets. Three samples were tested for each set.

## 3. Artificial neural networks

NNs which are inspired from performance of human's brain, are widely employed for analyzing complex problems and phenomena by means of functional relation. NNs have been used for modeling and analysis of non-linear processes which have different effective parameters as reported by (Maleki and Unal, 2020b). Schematic structure of a single layer NN fed with *r* and *s* number of input *p* and output *a* parameters respectively, with corresponded weight matrixes *w*, bias vectors *b*, linear combiner *u* and transfer function *f*, is presented in Fig. 2a.

Different SNNs and DNNs were developed via trial and error approach to achieve favorable NN with highest performance. 80% of data set (19 samples) was considered for training and the remained 20% (5 samples) was regarded for testing of the developed networks. In addition, a random function was used for selection of data for training and testing steps. Performance of the networks was determined in terms of the accuracy of the predicted results which assessed via correlation coefficient ($R^2$). $R^2$ can be calculated as follows (Maleki, 2015):

$$R^2 = \frac{\sum_{i=1}^{n}(f_{EXP,i} - F_{EXP})(f_{ANN,i} - F_{ANN})}{\sqrt{\sum_{i=1}^{n}\left((f_{EXP,i} - F_{EXP})^2 (f_{ANN,i} - F_{ANN})^2\right)}} \tag{1}$$

Where, $n$ is the number of fed samples, $f_{EXP}$ and $f_{ANN}$ represent the experimental and predicted values respectively. The values of $F_{EXP}$ and $F_{ANN}$ are determined as follows:

$$\boldsymbol{F_{EXP}} = \frac{1}{n}\sum_{i=1}^{n} \boldsymbol{f_{EXP,i}} \tag{2.a}$$

$$\boldsymbol{F_{ANN}} = \frac{1}{n}\sum_{i=1}^{n} \boldsymbol{f_{ANN,i}} \tag{2.b}$$

Fig. 2b and 2c reveal schematic illustration a typical SNN with two hidden layers and architecture of a SADDN respectively. Differences of SNN and SADNN and also the circumstance of developing them are mentioned in details by (E. Maleki et al., 2021b).

Fig. 2d indicates the considered inputs of developed networks including surface roughness, surface modification factor, surface hardness, surface residual stresses, relative density, yield strength and elongation. Also fatigue life was considered as the output of the developed networks. After obtaining optimum structures of NNs with highest accuracy and best performance, model function of the network which consists of the values of weights and biases was generated for further parametric and sensitivity analyses. The relevant model function in the SADNN with six layers can be generated as follows:

$$a^1 = f^1(w^1 i + b^1) \tag{3.a}$$

$$a^2 = f^2(w^2 i^1 + b^2) \tag{3.b}$$

$$a^3 = f^3(w^3 i^2 + b^3) \tag{3.c}$$

$$a^4 = f^4(w^4 i^3 + b^4) \tag{3.d}$$

$$a^5 = f^5(w^5 i^4 + b^5) \tag{3.f}$$

$$a^6 = M(m(1)) = f^6(w^6 i^5 + b^6) = f^6(w^6 f^5(w^5 f^4 (w^4 f^3 (w^3 f^2(w^2 f^1(w^1 i + b^1) + b^2) + b^3) + b^4) + b^5) + b^6) \tag{4}$$

Where $a^1$, $a^2$, $a^3$, $a^4$ and $a^5$ are the outputs of the first to fifth layers respectively. The function $M$ assigns the values of the considered seven input parameters of to the output parameter of fatigue life $m(1)$.

## 4. Results and discussions

Different analyses using OM and EBSD were carried out for microstructural characterization of the LPBF AlSi10Mg. Fig. 3a represents the OM microstructural observations of AB and AB+HT samples respectively in transversal (*xy*-plane) and longitudinal (*yz*-plane) cross sections. In longitudinal section of AB, the melt pool morphologies and hatching lines are clear and elongated boundaries along the build direction can be seen. However micrographs from the transversal section of AB, exhibit the melt pool tracks and the inhomogeneous microstructure orientated following the 67° rotation strategy used between the latter layers. On the other hand, in the AB+HT samples melt pool morphologies and hatching traces are mostly become invisible leading to a notable homogeneity in both cross-sections.

In addition, spherical and irregular pores which caused by gas trapping and insufficient melting respectively can be observed in both AB and AB+HT states. In addition, due to the microstructure modification after HT, as reported by (Bagherifard et al., 2018), the tensile properties of AB material with

tensile strength of 273 MPa and 2.5 % elongation is changed to tensile strength of 201 MPa and elongation of 13 % in the AB+HT sample and the ductility of the material is enhanced.
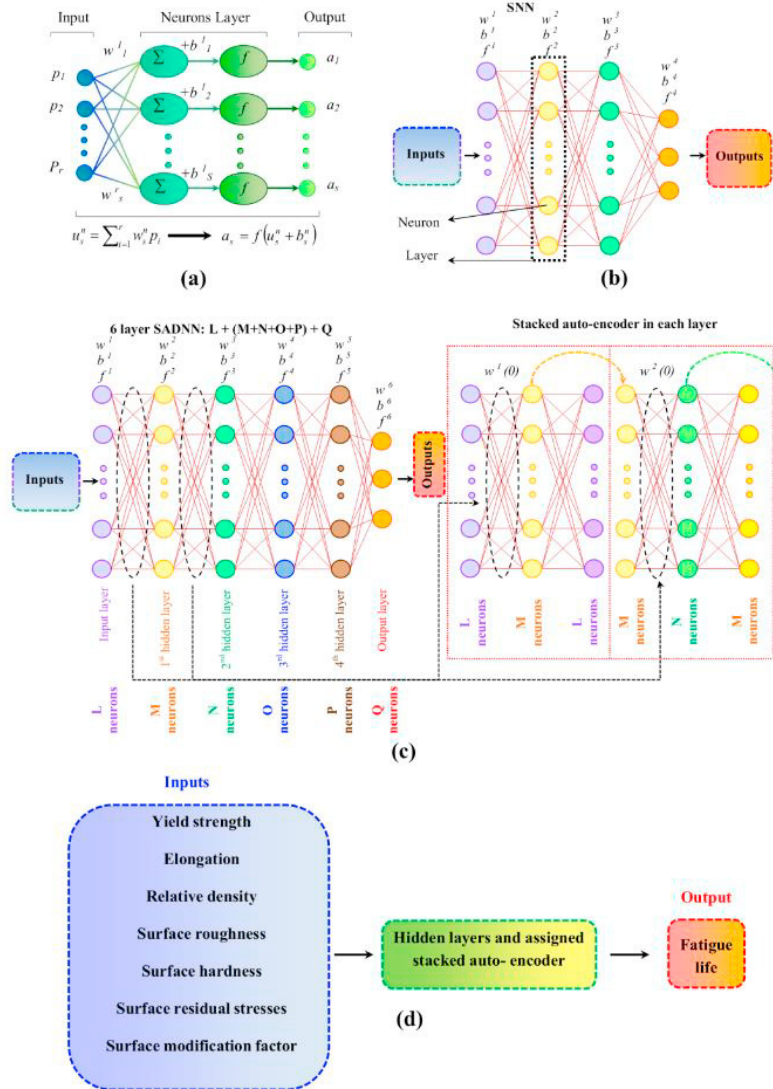


Fig. 2. Schematic illustration of: (a) a NN with one hidden layer considering the weight matrixes $w$, bias vectors $b$, linear combiner $u$ and transfer function $f$. (b) SNN with 4 layers and (c) DNN with 6 layers with the assigned SAE; adopted from (E. Maleki et al., 2021b; Erfan Maleki et al., 2021). (d) Corresponded input and out parameters used for modeling.

The porosity measurements were performed on all sets using image analysis of BSE-SEM observations in the notch area. Fig. 3b for instance illustrates the obtained BSE-SEM micrographs of the AB and AB+HT samples. The results indicated that after applying HT, porosity is slightly decreased. In addition sub-surface observations reveal that SP has no remarkable effects on reduction of porosities. Quantitative image analyses results indicate a range of 0.40-0.50 % porosity for all samples.

The results of different analyses of crystallographic orientation (IPF-$Z$), grain boundaries and geometrically necessary dislocation densities (GND) carried out by processing of the EBSD results in the shot peened surface layer of AB+SP and AB+Ht+SP samples are presented in Fig. 3d.

Transversal cross-section (*xy*-plane) along the building direction was conidered EBSD analyses. IPF-*Z* maps show the random and different orientation of the grains in the surface layer after SP compared to the dominant (001) orientation in the core material for both AB and AB+HT states. Grain boundaries with orientation of 2°< and 5°< were considered for processing the EBSD data. The grain boundary graphs reveal higher density of grain boundaries in the top surface layer comapred to the interior area which confirm the presence of gradiant microstructures on both AB+SP and AB+HT+SP sets starting with grians with size of lower than 0.5 µm on the top gradually enhancing to reach the original grain size at subsurface. In addition, GND values (as a factor dislocation densities) can be used as an index of plastic defrmation. In both AB+SP and AB+HT+SP sets, most concentrations and highest values of GND are observed in the top surface layer which confirms higher densities of refined grains in the mentioned area**.**
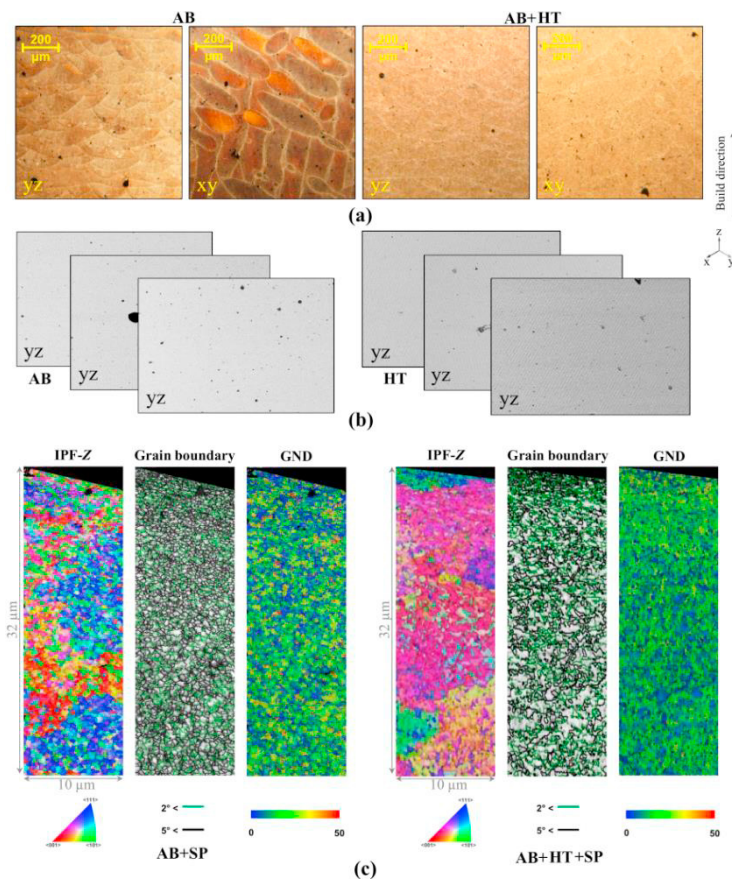


Fig. 3. (a) OM micrographs representing the microstructure of the AB and AB+HT samples in transversal and longitudinal cross-sections; adopted from (Maleki et al., 2022). (b) BSE-SEM observations in the notch area in the AB and AB+HT samples. (c) EBSD analyses in terms of IPF-Z, grain boundary and GND for AB+SP and AB+HT+SP samples.

Fig. 4 depicts the SEM micrographs taken from the notch area in AB, AB+SP and AB+SP+ECP samples. In the notch area of AB sample very poor surface quality can be observed clearly. In this area, three distinct regions of upward face, notch root and downwards face can be specified with particular surface morphologies and features. The qualitative comparison shows the lowest surface quality for the downward face with a high density of surface irregularities followed by the notch root and then the upward face. However, in the AB+SP sample, a modified surface morphology can be seen by applying

the plastic deformation and removing the partially melted and unmelted powders. Whereas, in the AB+SP+ECP sample, higher surface morphology modification can be seen and even the dimples formed by SP are mostly removed and almost all of the surface imperfections existed in the as-built and shot peened states were eliminated. The results indicate that AB+SP+ECP sample has the highest surface quality followed by AB+SP and AB samples respectively. This trend is also, observed in the heat treated samples.

In this study, rather than surface roughness values, new parameter of surface modification factor is presented as an index of effectiveness of each post-treatment on surface quality of the AM material. On the other hand, in implementation of ANN for modeling a phenomenon, the input data, should be normalized before feeding to the network. One of the standard normalizing methods is to divide the values of each input parameters to the highest value in the corresponding data set. In this way, all the data used for developing the network will place in the range of 0-1 (Maleki et al., 2020). Therefore, in order to develop the surface modification factor, a numeric criterion ranging from 0 to 1, was considered to describe the increasing of the surface quality after applying each treatments (see Fig. 4)
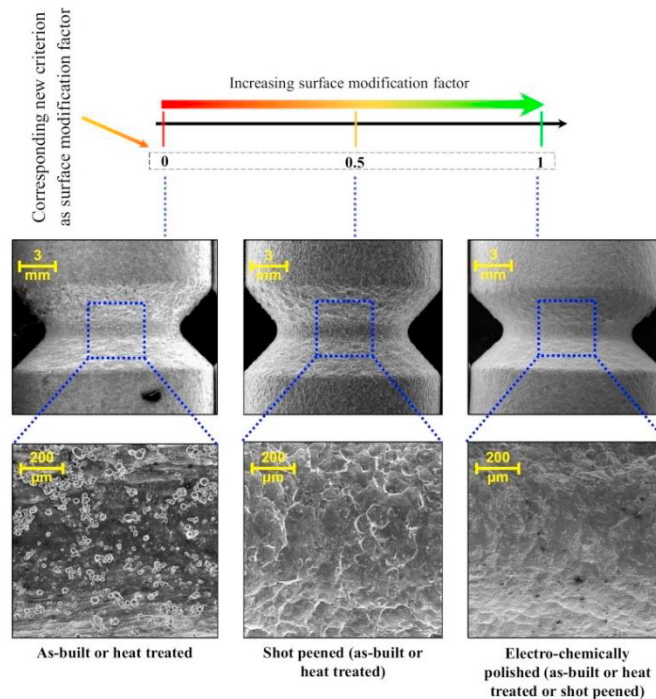


Fig. 4. Surface morphology of the AB, AB+SP and AB+SP+ECP samples and circumstance of assigning new criterion as surface modification factor.

After performing microstructural characterization and surface morphologies observations and also description of surface modification factor, other surface and mechanical properties including relative density, surface roughness, surface hardness and surface residual stresses were measured and obtained as well as the number of fatigue life cycles of each sets at fixed stress amplitude of 110 MPa. The obtained results for mentioned parameters are listed in Table 2. The results indicate that SP has remarkable effects on increasing of surface hardness and surface compressive residual stress. Considering surface properties, it can be seen that although the value of surface roughness parameter is slightly increased after SP, but modified surface morphology can be obtained. Also, it can be seen that ECP is considerably reduced the surface roughness.

Dealing with fatigue behaviour, the results indicate remarkable fatigue life improvement can be obtained after applying all considered post-treatments together and AB+HT+SP+ECP sample with about $4.3\times10^{6}$ cycles of fatigue life has more than 340 times higher life than AB sample. Also, considering the sole effects of each post-treatment, SP has the highest effect on fatigue behaviour improvement thanks to surface layer hardening, inducing high compressive residual stresses and surface morphology modification followed by ECP (due to very high surface modification and reducing surface roughness) and HT (due to microstructural homogenization) treatments.

Table 2. Obtained experimental results in terms of input and output parameters for each sets

| Sample No. | Sample set | Yield strength (MPa) | Elongation (%) | Relative density (%) | Surface roughness, Ra (μm) | Surface hardness (Hv) | Surface residual stress (MPa) | Surface modification factor | Fatigue life (Cycles) |
|---|---|---|---|---|---|---|---|---|---|
| 1 | AB | 273 | 2.5 | 99.6 | 4.5 | 120.7 | -5 | 0 | 13284 |
| 2 | | 273 | 2.5 | 99.6 | 4.5 | 120.7 | -5 | 0 | 10600 |
| 3 | | 273 | 2.5 | 99.6 | 4.5 | 120.7 | -5 | 0 | 14200 |
| 4 | AB+HT | 201 | 13 | 99.65 | 4.4 | 78.2 | -30 | 0 | 25200 |
| 5 | | 201 | 13 | 99.65 | 4.4 | 78.2 | -30 | 0 | 22100 |
| 6 | | 201 | 13 | 99.65 | 4.4 | 78.2 | -30 | 0 | 27030 |
| 7 | AB+SP | 273 | 2.5 | 99.62 | 4.6 | 156.2 | -83.5 | 0.5 | 1200200 |
| 8 | | 273 | 2.5 | 99.62 | 4.6 | 156.2 | -83.5 | 0.5 | 1300010 |
| 9 | | 273 | 2.5 | 99.62 | 4.6 | 156.2 | -83.5 | 0.5 | 1089200 |
| 10 | AB+HT+SP | 201 | 13 | 99.64 | 6.6 | 109 | -46.6 | 0.5 | 1978500 |
| 11 | | 201 | 13 | 99.64 | 6.6 | 109 | -46.6 | 0.5 | 2142000 |
| 12 | | 201 | 13 | 99.64 | 6.6 | 109 | -46.6 | 0.5 | 1920000 |
| 13 | AB+ECP | 273 | 2.5 | 99.51 | 2.9 | 120.2 | -4 | 1 | 200600 |
| 14 | | 273 | 2.5 | 99.51 | 2.9 | 120.2 | -4 | 1 | 234400 |
| 15 | | 273 | 2.5 | 99.51 | 2.9 | 120.2 | -4 | 1 | 210100 |
| 16 | AB+HT+ECP | 201 | 13 | 99.61 | 2.6 | 78 | -28.7 | 1 | 485600 |
| 17 | | 201 | 13 | 99.61 | 2.6 | 78 | -28.7 | 1 | 509800 |
| 18 | | 201 | 13 | 99.61 | 2.6 | 78 | -28.7 | 1 | 462800 |
| 19 | AB+SP+ECP | 273 | 2.5 | 99.57 | 3.2 | 150 | -79.2 | 1 | 3456000 |
| 20 | | 273 | 2.5 | 99.57 | 3.2 | 150 | -79.2 | 1 | 3700400 |
| 21 | | 273 | 2.5 | 99.57 | 3.2 | 150 | -79.2 | 1 | 3879010 |
| 22 | AB+HT+SP+ECP | 201 | 13 | 99.63 | 4.1 | 103 | -45.1 | 1 | 4210800 |
| 23 | | 201 | 13 | 99.63 | 4.1 | 103 | -45.1 | 1 | 3978890 |
| 24 | | 201 | 13 | 99.63 | 4.1 | 103 | -45.1 | 1 | 4430000 |

After achieving the experimental results and arranging them according to considered input and output parameters, different NNs were developed for modeling of the fatigue behavior of notched AlSi10Mg LPBF samples. In order to obtain a NN structure with highest performance and efficiency of several networks with different architecture and network parameters including SNN, DNN and SADNN were assessed and compared. Accuracy of the results in terms of output parameter of fatigue life were gathered from implemented SNNs with 1 and 2 hidden layers as a function of neurons' number in each layer as shown in Fig. 5a. It can be seen that by increasing the number of neurons in each considered layer, the accuracy of the SNNs are enhanced as well.

Fig. 5b compares the accuracy of the estimated fatigue life using SNNs, DNNs and SADNNs. In all of the developed networks, 7 and 1 neurons were respectively employed for input and output layers. In addition, in whole cases, learning rate of 0.185 was considered and a Logarithmic-Sigmod transfer function was used in both hidden and output layers. The results indicate that SADNN with a structure of 7+(24+20+10+4)+1 exhibited the highest performance among all the developed NNs, showing accuracies

of 0.99 and 0.96 for training and testing processes, respectively. Also, it can be seen that by increasing the depth of the NNS (by enhancing the number of layers) the accuracy enhances as well and pre-training process using stacked auto-encoder can remarkably increase the performance of the SADNN.

Having validated the high performance of the constructed SADNN, the relevant model function was generated for senesitivity and parametric analyses to evaluate the contribution of each input paramters on fatigue behavior of the notched AlSi10Mg LPBF samples.

Fig. 5c depicts the results obtained from sensitivity analysis. The analysis confirms that all the considered input parameters for the developed SADNN, directly affect the fatigue behavior. Fatigue behavior was found to be more sensitive to surface modification factor as most of the fatigue failures initiate from surface of the materials followed by elongation as an index of ductility of the material, surface residual stresses, surface hardness, yield strength of the material and surface roughness as well as relative density respectively.

Parametric analysis was carried out considering two most important input parameters of surface modification factor and elongation of the material (which obtained by sensitivity analysis) on fatigue behavior of the notched AlSi10Mg LPBF samples. For each parameter whole interval of experimnetal data was considered to achieve general case of the paramteric analysis. Fig. 5d depicts the 2D contour of the paramteric analysis in terms of surface modification factor and elongation of the material for analyzing the fatigue behavior. It can be seen that by enhacing surface modification factor by performing SP and especially ECP and also by applying HT to increase the elongation and therefore ductility of the material, the fatigue behavior of the  the notched AlSi10Mg LPBF samples are increased as well.
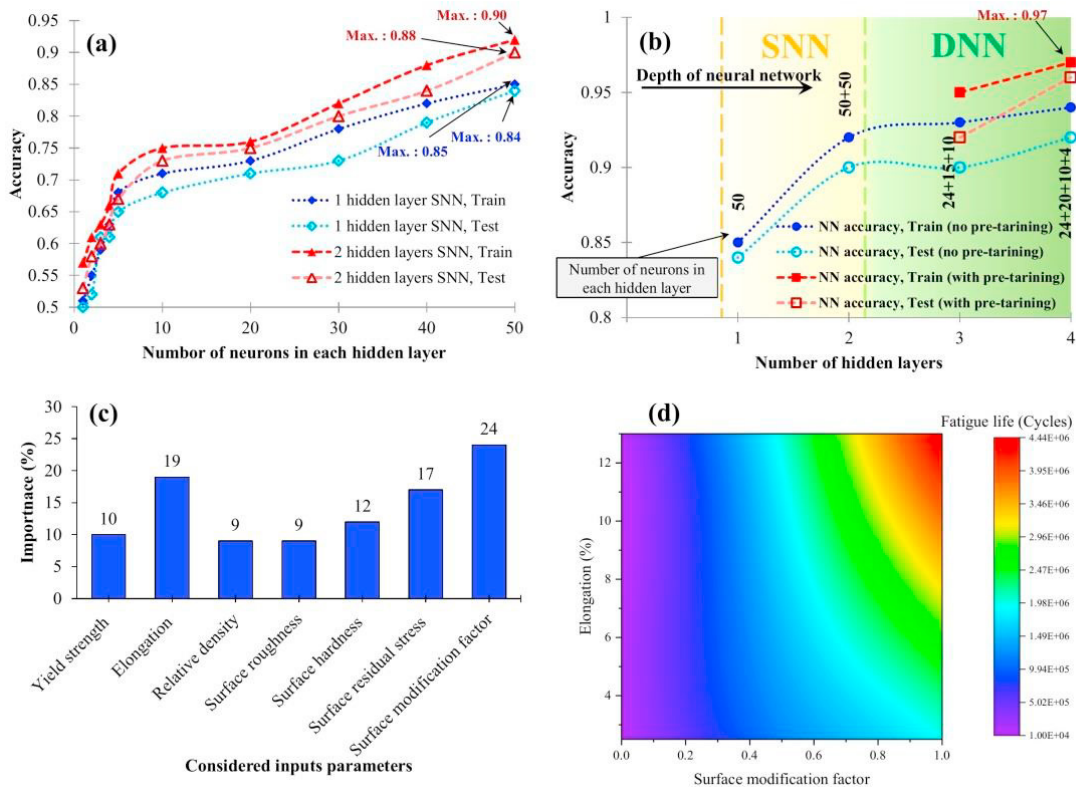


Fig. 5. (a) The effects of number of neurons in each layer of SNNs vs. accuracy of fatigue life estimation (b) Comparison of the fatigue life estimation accuracy between developed NNs of different structures including SNN, DNN and SADNN. Obtained results of (c) sensitivity and (d) parametric analyses.

## 5. Conclusions

In this study, firstly the effects of four different post-treatments including HT, SP and ECP treatments as well as their combination as hybrid treatments, on microstructure, mechanical properties and fatigue behavior of LPBF V-notched AlSi10Mg samples were experimentally investigated. Comprehensive experimental tests including microstructural characterization, porosity and surface morphology analyses as well as mechanical characterization including hardness and residual stresses measurement and rotating bending fatigue tests were performed on the as-built and heat treated samples before and after applying SP and ECP treatments. Then, an alternative approach using deep learning was employed for modelling the fatigue behaviour through artificial neural network. Surface roughness, surface modification factor, surface hardness, surface residual stresses, relative density, yield strength and elongation were considered as inputs and fatigue life was regarded as the output of the developed network. NN modelling was performed by developing different SNN, DNN and SADNN neural networks. Based on the obtained results the following conclusions can be drawn:

- Very poor surface quality was observed in the as-built state.
- HT considerably modified and homogenized the inhomogeneous microstructure of the as-built state.
- Surface layer grain refinement leading to a gradient microstructure was obtained after applying SP treatments. In addition SP modified the surface morphology of the as-built and heat treated samples as well as surface layer hardening and inducing high compressive residual stresses.
- ECP efficiently eliminated the surface imperfections of the as-built and other treated samples and reduced the surface roughness.
- All applied post-treatments improved the fatigue behavior of the notched samples. Considering sole influence of each post-treatment, SP has the highest effect followed by ECP and HT on fatigue life improvement.
- Comparing the accuracy of the obtained output of the developed networks indicated that pre-trained SADNN exhibited the highest performance.
- Sensitivity analysis showed that surface modification factor followed by elongation, surface residual stresses, surface hardness, yield strength of the material and surface roughness as well as the relative density have the highest importance on fatigue life improvement, respectively.
- Parametric analysis revealed that surface modification factor by performing SP and especially ECP and also by applying HT to increase ductility of the material, the fatigue behavior of the notched AlSi10Mg LPBF samples are increased as well.
- AI based methods such as deep learning with pre-training methods such as stacked auto-encoder can be used as a powerful tool for analyzing the fatigue behavior of the as-built and post-treated additively manufactured materials.

### References

AlMangour, B., Yang, J.M., 2016. Improving the surface quality and mechanical properties by shot-peening of 17-4 stainless steel fabricated by additive manufacturing. Mater. Des. https://doi.org/10.1016/j.matdes.2016.08.037

Bagherifard, S., Beretta, N., Monti, S., Riccio, M., Bandini, M., Guagliano, M., 2018. On the fatigue strength enhancement of additive manufactured AlSi10Mg parts by mechanical and thermal post-processing. Mater. Des. 145, 28–41. https://doi.org/10.1016/j.matdes.2018.02.055

Balachandramurthi, A.R., Moverare, J., Dixit, N., Pederson, R., 2018. Influence of defects and as-built surface roughness on fatigue properties of additively manufactured Alloy 718. Mater. Sci. Eng. A. https://doi.org/10.1016/j.msea.2018.08.072

Bengio, Y., Lamblin, P., Popovici, D., Larochelle, H., 2007. Greedy layer-wise training of deep networks, in: Advances in Neural Information Processing Systems. https://doi.org/10.7551/mitpress/7503.003.0024

Chen, J., Liu, Y., 2021. Fatigue property prediction of additively manufactured Ti-6Al-4V using probabilistic physics-guided learning. Addit. Manuf. https://doi.org/10.1016/j.addma.2021.101876

DebRoy, T., Wei, H.L., Zuback, J.S., Mukherjee, T., Elmer, J.W., Milewski, J.O., Beese, A.M., Wilson-Heid, A., De, A., Zhang, W., 2018. Additive manufacturing of metallic components – Process, structure and properties. Prog. Mater. Sci. https://doi.org/10.1016/j.pmatsci.2017.10.001

EN ISO 4287, 1997. Geometrical Product Specifications (GPS) - Surface texture: Profile method - Terms, definitions and surface texture parameters. Int. Organ. Stand.

Feng, S., Zhou, H., Dong, H., 2019. Using deep neural network with small dataset to predict material defects. Mater. Des. 162, 300–310. https://doi.org/10.1016/j.matdes.2018.11.060

Ferro, P., Fabrizi, A., Berto, F., Savio, G., Meneghello, R., Rosso, S., 2020. Defects as a root cause of fatigue weakening of additively manufactured AlSi10Mg components. Theor. Appl. Fract. Mech. https://doi.org/10.1016/j.tafmec.2020.102611

Gardan, J., 2016. Additive manufacturing technologies: State of the art and trends. Int. J. Prod. Res. https://doi.org/10.1080/00207543.2015.1115909

Hamidi Nasab, M., Gastaldi, D., Lecis, N.F., Vedani, M., 2018. On morphological surface features of the parts printed by selective laser melting (SLM). Addit. Manuf. https://doi.org/10.1016/j.addma.2018.10.011

Herzog, D., Seyda, V., Wycisk, E., Emmelmann, C., 2016. Additive manufacturing of metals. Acta Mater. https://doi.org/10.1016/j.actamat.2016.07.019

Hinton, G.E., Osindero, S., Teh, Y.W., 2006. A fast learning algorithm for deep belief nets. Neural Comput. https://doi.org/10.1162/neco.2006.18.7.1527

Hinton, G.E., Salakhutdinov, R.R., 2006. Reducing the dimensionality of data with neural networks. Science (80-. ). https://doi.org/10.1126/science.1127647

Lewandowski, J.J., Seifi, M., 2016. Metal Additive Manufacturing: A Review of Mechanical Properties. Annu. Rev. Mater. Res. https://doi.org/10.1146/annurev-matsci-070115-032024

Li, R., Liu, J., Shi, Y., Wang, L., Jiang, W., 2012. Balling behavior of stainless steel and nickel powder during selective laser melting process. Int. J. Adv. Manuf. Technol. https://doi.org/10.1007/s00170-011-3566-1

Liu, G., Bao, H., Han, B., 2018. A Stacked Autoencoder-Based Deep Neural Network for Achieving Gearbox Fault Diagnosis. Math. Probl. Eng. https://doi.org/10.1155/2018/5105709

Livingstone, D.J., Manallack, D.T., Tetko, I. V., 1997. Data modelling with neural networks: Advantages and limitations. J. Comput. Aided. Mol. Des. https://doi.org/10.1023/A:1008074223811

Maleki, E., 2015. Artificial neural networks application for modeling of friction stir welding effects on mechanical properties of 7075-T6 aluminum alloy, in: IOP Conference Series: Materials Science and Engineering. https://doi.org/10.1088/1757-899X/103/1/012034

Maleki, E., Bagherifard, S., Bandini, M., Guagliano, M., 2021a. Surface post-treatments for metal additive manufacturing: Progress, challenges, and opportunities. Addit. Manuf. 37, 101619. https://doi.org/10.1016/j.addma.2020.101619

Maleki, Erfan, Bagherifard, S., Guagliano, M., 2021. Application of artificial intelligence to optimize the process parameters effects on tensile properties of Ti-6Al-4V fabricated by laser powder-bed fusion. Int. J. Mech. Mater. Des. https://doi.org/10.1007/s10999-021-09570-w

Maleki, E., Bagherifard, S., Razavi, S.M.J., Riccio, M., Bandini, M., du Plessis, A., Berto, F., Guagliano, M., 2022. Fatigue behaviour of notched laser powder bed fusion AlSi10Mg after thermal and mechanical surface post-processing. Mater. Sci. Eng. A 829, 142145. https://doi.org/10.1016/j.msea.2021.142145

Maleki, E., Farrahi, G.H.H., 2018. Modelling of conventional and severe shot peening influence on properties of high carbon steel via artificial neural network. Int. J. Eng. Trans. B Appl. 31. https://doi.org/10.5829/ije.2017.30.11b.00

Maleki, E., Mirzaali, M.J., Guagliano, M., Bagherifard, S., 2020. Analyzing the mechano-bactericidal effect of nano-patterned surfaces on different bacteria species. Surf. Coatings Technol. https://doi.org/10.1016/j.surfcoat.2020.126782

Maleki, E., Unal, O., 2020a. Optimization of Shot Peening Effective Parameters on Surface Hardness Improvement. Met. Mater. Int. https://doi.org/10.1007/s12540-020-00758-x

Maleki, E., Unal, O., 2020b. Fatigue limit prediction and analysis of nano-structured AISI 304 steel by severe shot

peening via ANN. Eng. Comput. https://doi.org/10.1007/s00366-020-00964-6

Maleki, E., Unal, O., 2019. Shot Peening Process Effects on Metallurgical and Mechanical Properties of 316 L Steel via: Experimental and Neural Network Modeling. Met. Mater. Int. https://doi.org/10.1007/s12540-019-00448-3

Maleki, E., Unal, O., Guagliano, M., Bagherifard, S., 2021b. Analysing the Fatigue Behaviour and Residual Stress Relaxation of Gradient Nano-structured 316L Steel Subjected to the Shot Peening via Deep Learning Approach. Met. Mater. Int. https://doi.org/https://doi.org/10.1007/s12540-021-00995-8

Maleki, E., Unal, O., Guagliano, M., Bagherifard, S., 2021c. The effects of shot peening, laser shock peening and ultrasonic nanocrystal surface modification on the fatigue strength of Inconel 718. Mater. Sci. Eng. A 810. https://doi.org/10.1016/j.msea.2021.141029

Maleki, E., Unal, O., Reza Kashyzadeh, K., 2018. Fatigue behavior prediction and analysis of shot peened mild carbon steels. Int. J. Fatigue 116, 48–67. https://doi.org/10.1016/j.ijfatigue.2018.06.004

Maleki, N., Kashanian, S., Maleki, E., Nazari, M., 2017. A novel enzyme based biosensor for catechol detection in water samples using artificial neural network. Biochem. Eng. J. 128, 1–11. https://doi.org/10.1016/j.bej.2017.09.005

Maleki, N., Maleki, E., 2015. Modeling of cathode Pt /C electrocatalyst degradation and performance of a PEMFC using artificial neural network, in: ACM International Conference Proceeding Series. https://doi.org/10.1145/2832987.2833000

Mfusi, B.J., Mathe, N.R., Tshabalala, L.C., Popoola, P.A.I., 2019. The effect of stress relief on the mechanical and fatigue properties of additively manufactured AlSi10Mg parts. Metals (Basel). https://doi.org/10.3390/met9111216

Mukherjee, T., Zhang, W., DebRoy, T., 2017. An improved prediction of residual stresses and distortion in additive manufacturing. Comput. Mater. Sci. https://doi.org/10.1016/j.commatsci.2016.10.003

Qi, X., Chen, G., Li, Y., Cheng, X., Li, C., 2019. Applying Neural-Network-Based Machine Learning to Additive Manufacturing: Current Applications, Challenges, and Future Perspectives. Engineering 5, 721–729. https://doi.org/10.1016/j.eng.2019.04.012

SAE International, 2010. SAE J443: Procedures for Using Standard Shot Peening Almen Strip. Surf. Veh. Recomm. Pract.

Sames, W.J., List, F.A., Pannala, S., Dehoff, R.R., Babu, S.S., 2016. The metallurgy and processing science of metal additive manufacturing. Int. Mater. Rev. https://doi.org/10.1080/09506608.2015.1116649

Schneider, C.A., Rasband, W.S., Eliceiri, K.W., 2012. NIH Image to ImageJ: 25 years of image analysis. Nat. Methods. https://doi.org/10.1038/nmeth.2089

Wang, Y. Bin, You, Z.H., Li, X., Jiang, T.H., Chen, X., Zhou, X., Wang, L., 2017. Predicting protein-protein interactions from protein sequences by a stacked sparse autoencoder deep neural network. Mol. Biosyst. https://doi.org/10.1039/c7mb00188f

Yadroitsev, I., Smurov, I., 2011. Surface morphology in selective laser melting of metal powders, in: Physics Procedia. https://doi.org/10.1016/j.phpro.2011.03.034

Zhan, Z., Li, H., 2021. Machine learning based fatigue life prediction with effects of additive manufacturing process parameters for printed SS 316L. Int. J. Fatigue. https://doi.org/10.1016/j.ijfatigue.2020.105941

Zhang, Z., Sun, C., Xu, X., Liu, L., 2018. Surface quality and forming characteristics of thin-wall aluminium alloy parts manufactured by laser assisted MIG arc additive manufacturing. Int. J. Light. Mater. Manuf. https://doi.org/10.1016/j.ijlmm.2018.03.005